Briefings in Bioinformatics, 2026, 27, bbag135
https://doi.org/10.1093/bib/bbag135
Published: 28 March 2026
Case Study

OXFORD

Spotting a unicorn: spatial transcriptome analysis of the eyelid reveals gene regulatory networks enriched in Moll glands

Tomas Konecny [1,2], Hans Binder [1,2], Ulrike Hampel [3], Florian Hansmann [4], Helga Pfannkuche [5], Marlon R. Schneider [5,*]

[1]Interdisciplinary Centre for Bioinformatics (IZBI), University of Leipzig, Härtelstr. 16-18, 04107 Leipzig, Germany
[2]Armenian Bioinformatics Institute (ABI), 7 Ezras Hasratyan St, 0014 Yerevan, Armenia
[3]Department of Ophthalmology, University Hospital Leipzig, Liebigstraβe 10-14, 04103 Leipzig, Germany
[4]Institute of Veterinary Pathology, Veterinary Faculty, University of Leipzig, An den Tierkliniken 33, 04103 Leipzig, Germany
[5]Institute of Veterinary Physiology, Veterinary Faculty, University of Leipzig, An den Tierkliniken 7, 04103 Leipzig, Germany

*Corresponding author. Institute of Veterinary Physiology, University of Leipzig, An den Tierkliniken 7, 04103 Leipzig, Germany. E-mail: marlon.schneider@vetmed.uni-leipzig.de
Marlon R. Schneider is a Professor of Physiology at the Faculty of Veterinary Medicine, Leipzig University

Abstract

Moll glands, found in the margin of the eyelid next to the base of the eyelashes, are likely to play an important role in maintaining the tear film and therefore in securing adequate visual function. However, information about their secretion and its regulation is extremely scarce. Here, we subjected spatial transcriptome data of the human eyelid to bioinformatics workflows incorporating machine learning to shed light on the Moll-specific transcriptional program. We identified Moll-specific genes such as HPD, CYP4Z1, PIP, GLYATL2, or SCGB2A2, which delineate a transcriptional core, i.e. not shared with other eyelid elements. Gene ontology enrichment analyses further depicted the biological functions of the Moll gland transcriptional programs, which include tyrosine metabolism and biosynthesis, extracellular exosome, small molecule metabolism, and erythrose 4-phosphate/phosphoenolpyruvate-family amino acid metabolism. Expression of GLYATL2 and HPD, identified as a specific and sensitive transcripts in the Moll gland transcriptome, was confirmed by immunofluorescence in the eyelid of four different patients, thus supporting the validity of our approach. Collectively, these results indicate that Moll-associated gene sets exhibit distinct but complementary functional programs, reflecting the gland's specialized metabolic capacity and secretory function within the eyelid tissue microenvironment. Our study provides the first in-depth analysis of the human Moll gland transcriptional landscape and identifies novel targets for regulating Moll gland homeostasis in health and disease.

Keywords **eyelid, Moll gland, spatial transcriptomics, self-organizing map portrayal**

Introduction

The tear film is a complex extracellular fluid with essential functions in maintaining high quality vision, preventing infection, suppressing inflammation, healing injuries, and clearing debris from the surface of the eye [1]. It has a highly intricate composition, including water, electrolytes, mucins, and numerous proteins and lipids. Tear film production, delivery and regulation are brought about by the lacrimal functional unit (LFU), which includes the lacrimal glands, the ocular surface, and the eyelids with their associated glands (accessory lacrimal glands, Meibomian glands and others). Accordingly, dysfunction in any component of the LFU can cause tear film instability, inflammation and ocular disorders leading to impaired visual function.

Recently, methods such as single cell-sequencing and spatial transcriptomics in association with innovative downstream bioinformatic analysis significantly expanded our knowledge about the gene networks regulating the activity of lacrimal [2, 3] and Meibomian glands [4–7]. However, other glandular structures of the eyelid, such as the Krause, Moll, or Zeis glands have received less attention, despite their critical role in maintaining the tear film stability and providing antimicrobial defense. This is particularly true for the apocrine Moll glands, also known as ciliary or eyelash glands. As they are found in association with every eyelash, they are localized over the entire eyelid margin, a component of the LFU with critical functions for the ocular surface integrity [8]. Intriguingly, as highlighted by a recent and comprehensive review article [9], our knowledge about the Moll gland is extremely scarce, and essentially restricted to their morphology

Received: November 6, 2025. **Revised:** January 27, 2026. **Accepted:** February 28, 2026

and the identity of a few membrane proteins [10, 11] and secretion products [12, 13].

From a methodological perspective, spatial transcriptomics of skin glands enables the systematic analysis of transcriptional programs within microanatomical structures composed of only a few cell layers, while preserving their spatial context. When combined with advanced computational analysis, these data allow the extraction of spatially resolved gene expression patterns that are not readily apparent from bulk or single cell expression values alone. In this study, we employ an analytical approach that complements the "microscopy of gene expression" with a comprehensive machine learning framework known as molecular portrayal, based on self-organizing maps (SOM). This approach enables the integration, visualization, segmentation, and functional knowledge mining of complex spatial transcriptomics data, facilitating the identification of spatially coherent transcriptional modules at single spot resolution [14, 15]. While the method requires careful parameterization and interpretation, it provides an efficient way to dissect gland-specific transcriptional programs in complex tissues. Here, we present a case study demonstrating the application of this approach to investigate the transcriptional program specifically activated in the Moll gland, extending our previous analysis of the Meibomian and Zeis glands of the eyelid [7].

Our in-depth analysis pinpoints transcripts and pathways determining Moll cellular function. Our approach enables us to identify a number of previously unknown Moll gland markers that may be useful for future studies on the biology and pathology of these understudied eyelid glands. SOM portrayal of spatial transcriptomics data in combination with specificity analysis applied here provides an option to discover microanatomical structures in spatial transcriptomics beyond this case study.

Materials and methods

Tissue sampling and spatial transcriptomics

The collection and analysis of the eyelid sample were approved by the ethics committee of the medical faculty of the University of Leipzig (070–22-ek). The eyelid samples employed in this study were collected at the Department of Ophthalmology of the University of Leipzig during lateral tarsal strip procedure for ectropion correction and after patient consent for use of the specimen for research purposes, and in full compliance with the Declaration of Helsinki principles. The patients were three men aged 60 years (patient 1), 76 years (patient 3), and 71 years (patient 4), as well as a women aged 72 years (patient 2). Patient 1 was employed for the spatial transcriptome analysis; all four patients were employed for immunofluorescence staining. The sample was formalin-fixed, paraffin-embedded, and spatial transcriptomic analysis was carried out using 10X Genomics Visium technology as described previously [7].

Processing of spatial transcriptomics data

The spatial transcriptomics dataset comprises 3902 observations/spots and 15 801 genes. Each observation includes spatial coordinates and tissue identity. Genes expressed in fewer than three spots were filtered out. No reference based deconvolution was performed due to lack of a matched single cell reference. For clustering on spatial transcriptomics data, the Leiden algorithm was used, as implemented in the scanpy Python package (version 1.11.4; Python version 3.11.13) using "scanpy.tl.leiden" with parameter "resolution" = 0.5. The Leiden clusters were visualized using "scanpy.tl.umap" for dimensionality reduction and projection.

Identifying MOLL specific marker genes

The recognition of genes enriched in tissue clusters (spatial marker genes) was assessed by applying the Wilcoxon rank-sum test identifying genes that are significantly overexpressed in the Moll tissue cluster compared to other Leiden clusters [16]. A total of 63 ST-based MOLL marker genes, specific to the MOLL spot (i.e. associated with Moll gland tissue), with positive Wilcoxon score and adjusted *P*-values below .01 were retained.

For each MOLL marker gene, expression was compared between two groups, spots inside the MOLL region (inMOLL) and spots outside it (outMOLL), i.e. in any of the other tissue spots. Two differential measures inMOLL versus outMOLL were calculated:

(i) how strongly a gene G is differentially expressed (expression ratio),

$$Expression\ ratio_{MOLL}\,[G] = \log_2\left(\frac{inMOLL_{AVG\ EX}}{outMOLL_{AVG\ EX}}\right)$$

and (ii) how differently it appears as spot-related count (spot count ratio),

$$Spot\ count\ ratio_{MOLL}\,[G] = \frac{\#inMOLL_{UP} \times \#\ outMOLL}{\#\ inMOLL \times \#\ outMOLL_{UP}}$$

These measures were combined as product into a single score, termed MOLL specificity, which combines MOLL-specific overexpression and MOLL-specific spot abundance for gene G.

$$Specificity_{MOLL}\,[G] = Expression\ ratio_{MOLL}\,[G] \times Spot\ count\ ratio_{MOLL}\,[G]$$

Ranking genes according to their MOLL specificity score then provided candidates for markers of MOLL-related transcriptional programs.

Self-organizing maps tissue portrayal

SOM machine learning was applied to all spatial spots of the eyelid to generate a transcriptomic "portrait" of each of them [7] using oposSOM software [17]. SOM training was performed on all 3902 spots and 15 801 transcripts using a map size of 55×55 metagenes. All other settings followed the default criteria described in the original publication [17]. In brief, SOM training was performed on centralized, quantile-normalized, log-transformed expression data with standard settings of the machine learning algorithm (quadratic grid topology, deterministic linear initialization, 25 0000 iterations with decreasing learning rate, a gaussian neighborhood function and *Euclidean* similarity metrics) [18–20], which have been proven to provide robust results in previous applications including studies of spatial transcriptomics data [14, 15]. Mean tissue portraits were obtained by averaging over all spot portraits of the respective tissue. These portraits reveal modules of coexpressed genes overexpressed in the respective tissue as red areas which were then extracted by module segmentation as described previously [20]. Particularly, these modules were identified using the group overexpression method which first selects the top 10% of overexpressed metagenes in each of the tissue averaged group portraits and then module clusters were extracted as adjacent areas

of the selected metagenes. We considered genes of the MOLL module overexpressed almost exclusively in the MOLL spots, as well as tissue modules highly expressed in the Meibomian gland basal and differentiation layers (MEI) mostly associated with lipogenesis, another MEI-related module related to energy metabolism, in particular oxidative phosphorylation (OXPHOS) and a module upregulated in hair follicles (HF) related to RNA-processing (see below). An interactive version for browsing the data is provided under the link http://gondwanaland.izbi.uni-leipzig.de:5978/?dataset=17.

Selection of MOLL-related genes

Both MOLL-related marker genes (63 genes) as well as MOLL-module genes as identified using SOM portrayal (28 genes) provide a list of joint candidates for MOLL functions which is further extended by genes of SOM modules coexpressed in the MOLL-tissue (MEI, Oxphos and HF) (Fig. S1). Final filtering and stratification was then performed by gene overlap analysis using upsetplot (version 0.9.0) in its Python implementation [21].

Function mining

To functionally annotate the MOLL-associated Spatial Transcriptomics (ST) markers, we used gene set enrichment analysis as implemented in the oposSOM package [17, 19] and Gene Ontology (GO) enrichment analysis using the g:Profiler (g:GOSt) tool [22, 23] and the Search Tool for the Retrieval of Interacting Genes/Proteins database (STRING) database [24] with default settings. Input gene lists included the ST markers and their overlap with SOM-based MOLL module genes.

Immunofluorescence

For the detection of Glycine N-acyltransferase-like protein 2 (GLYATL2) and 4-Hydroxyphenylpyruvate Dioxygenase (HPD), 5 μm-thick tissue sections were deparaffinized, washed (3x3 min) in Tris-buffered saline (TBS), preincubated for 60 min in TBS containing 5% bovine serum albumin, and incubated overnight with primary rabbit-anti-GLYATL2 antibodies (dilution 1:100; ABIN7004275; antibodies-online, Aachen, Germany) or rabbit-anti-HPD antibodies (dilution 1:100; 17004-1-AP; Proteintech, Planegg-Martinsried, Germany). Next, the specimens were washed three times in TBS and incubated for 2.5 h at room temperature in buffer solution containing secondary anti-rabbit antibodies raised in goats conjugated to indocarbocyanine (Cy3, SA00009-2, Proteintech, Planegg–Martinsried, Germany) at a dilution of 1:500. To stain nuclei, sections were incubated for 1 min at room temperature with 4′,6-diamidin-2-phenylindole (DAPI, Sigma–Aldrich, Taufkirchen, Germany) at a dilution of 1:4000. Finally, the specimens were washed in TBS, coverslipped with Prolong Gold Antifade Mountant (P10144 Invitrogen, Darmstadt, Germany) and stored at 4 °C. To exclude fluorescent signals due to nonspecific binding of secondary antibodies, negative controls without primary antibodies were prepared.

The stained sections were analyzed using a fluorescence microscope (Zeiss Axio Observer 7 Apotome, Carl Zeiss, Jena, Germany). The employed objectives were EC Plan-Neofluar 10x/0.3 and Plan-Apochromat 20x/0.8 (both from Carl Zeiss, Jena, Germany). Photomicrographs were taken with a black and white camera (Axiocam 705 mono R2, Carl Zeiss, Jena, Germany) attached to an image analysis system (ZEN 3.6 blue edition, Carl Zeiss, Jena, Germany).

Results

The Moll gland shows a specific transcriptomic profile in the eyelid

Haematoxylin and eosin staining (H&E) of the eyelid distinguished Meibomian, sebaceous (Zeis) and Moll glands, thus enabling a comprehensive view of ocular adnexal tissue (Fig. 1A). Transcriptomic analysis revealed the presence of distinct epithelial, glandular, and immune compartments, each corresponding to specific anatomical entities as assessed by an experienced pathologist (F.H.) and ophtalmologist (U.H.) (Fig. 1B and C). Meibomian glands, sebaceous glands, HFs, dermis, and the gland of Moll are clearly separated, highlighting their specific transcriptional signatures (see also [7]). Mean SOM portrait averaged over that of the 41 ST-spots of the Moll gland indicates a specific "MOLL" module of 28 coregulated genes (Fig. 1E and F) virtually not expressed or only weakly expressed in any of the other tissue spots and weakly correlating with their respective expression modules (Fig. 1G and H). The mean SOM portrait of the MOLL modules also reveals other expression modules shared partly with the Meibomian gland (MEI) and associating with energy (oxidative phosphorylation) and lipid metabolism, and with other tissues such as the HF and the suprabasal epidermal layer (EPI-S) (Fig. 1E–H, Fig. S1) in agreement with diverse MOLL-related epidermal functions [9].

Hence, the spatial transcriptome image of the eyelid shows a well-defined region referred to the Moll gland expressing a series of specific genes as well as genes sharing expression with other tissues, first of all those of the MEI and HF spots.

Molecular signatures of the gland of Moll

Next, we were interested in identifying gene lists of different categories relevant for MOLL transcriptional programs. Here we consider (see also Materials and Methods and Fig. S2), (i) genes of the SOM-based MOLL module (Fig. 1E and F) and (ii) ST-based MOLL markers using Wilcoxon rank sum testing (63 genes). Both gene sets (i) and (ii) overlap in 10 genes marked in dark red (Fig. 2A–C). This first group included *ABCC11, ALPL, CYP4Z1, GLYATL2, HPD, KIAA1324, PIP, SCGB2A2, SPINK8*, and *TTC36* giving rise to gene-wise ST images showing their specific expression in the Moll gland which appears as well-separated entity (Fig. 2C). In other words, these "MOLL-only" genes highlight spatially restricted transcriptional programs that define the gland's individuality within the ocular landscape.

For an extended view we generated mutual overlaps between ST markers and genes of the co-expressed tissue modules upregulated in MEI, OXPHOS, and HF spots (Fig. 2B). Nine genes (*ALDH3B2, CYB5A, FASN, GPX4, MUC1, MUCL1, MYLK, NUPR1, PABPC1*) overlap between ST markers and MEI module and another eight genes combine in addition memberships of the HF and/or OXPHOS modules (*TFAP2B, EEF2, PILRB, RACK1*, *AFMID, SLC38A1, EIF4B*, and *DST*). Overall these genes upregulate in the MOLL spots, but also in other tissue spots of the eyelid (Fig. 2C and Fig. S2), which suggests shared functional categories such as key secretory and structural regulators, confirming that the gland maintains a unique balance between apocrine secretion and epithelial differentiation.

In summary, we identified MOLL-specific genes which delineate a transcriptional core, i.e. virtually not shared with other tissues of the eyelid, thereby establishing the molecular individuality of the gland of Moll. Partial intersections with MEI, OXPHOS, HF, and other modules, in contrast, contained conserved pathways involved in epithelial

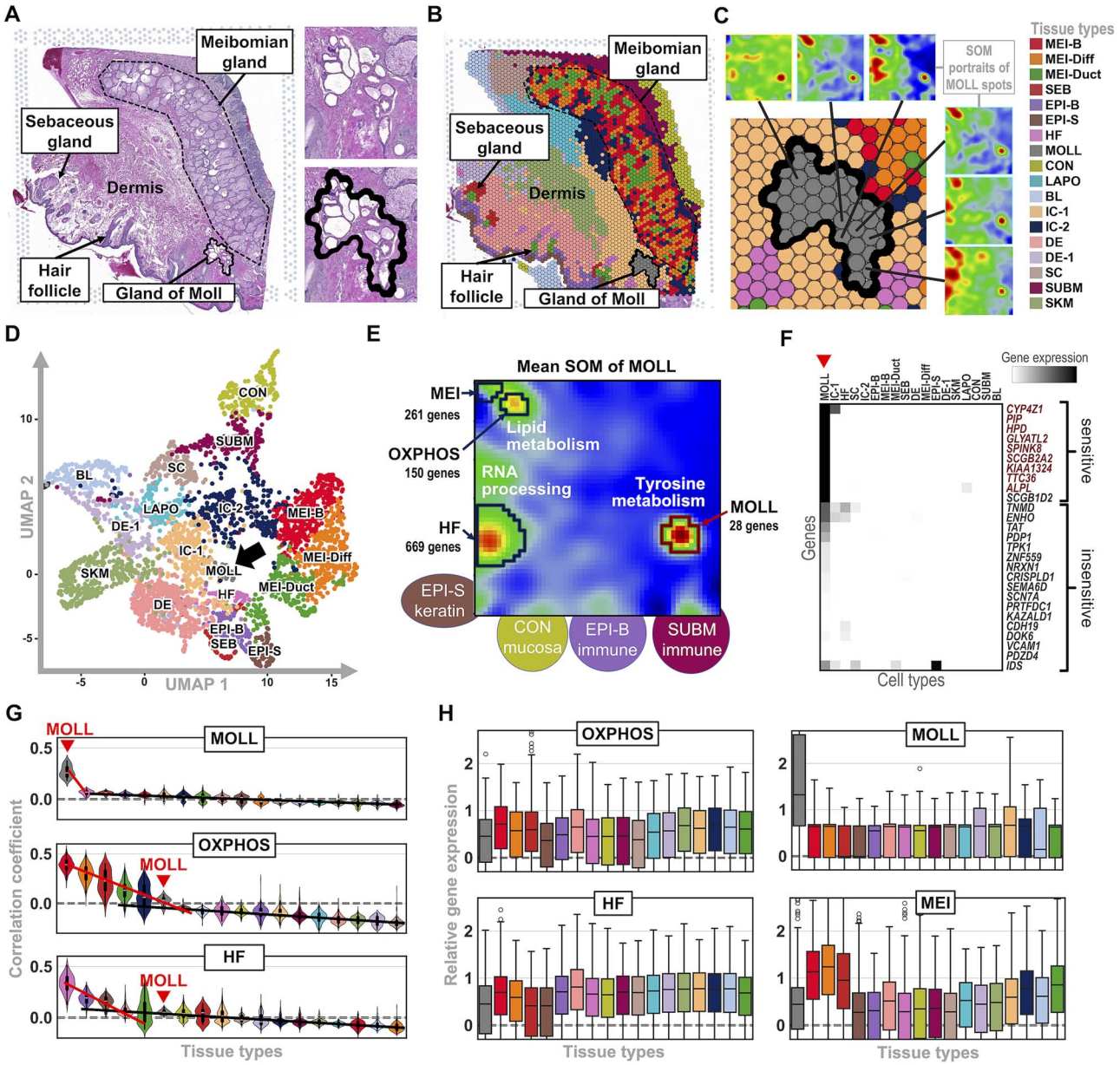

Figure 1 The spatial transcriptome of the eyelid reveals a specific gene expression signature of the Moll gland. H&E (A) and spatial transcriptomics (B) images of the eyelid. Higher magnification (C) detailing the area of the Moll gland also shows individual SOM portraits of selected ST spots. Assignments of the spots to different tissue types were obtained using Leiden clustering, as indicated in the spatial and (D) Uniform Manifold Approximation and Projection (UMAP) plots. (E) Mean SOM portrait of the MOLL spots obtained by averaging over all individual SOM portraits of the MOLL spots. It highlights modules of co-expressed genes corresponding to the MOLL spots and genes related to "OXPHOS" energy metabolism and RNA processing, upregulated in MEI and HF spots, respectively. Other modules refer to different tissue spots, as indicated. (F) Genes of the MOLL module are specifically activated in this region. (G) Boxplot showing the expression of selected expression modules across all tissue types. (H) Pearson's correlation coefficients of selected modules relative to all others indicate the specificity of the extracted genes as well as the most similar expression profiles in other tissue modules. Genes of the MOLL module virtually self-correlate only within the Moll tissue, whereas genes of the OXPHOS and HF modules moderately correlate with MEI and SEB spots and with EPI and HF spots, respectively. Meibomian gland basal cells (MEI-B), meibomian gland differentiated cells (MEI-DIFF), meibomian gland ductal cells (MEI-DUCT), sebaceous glands (SEB), hair follicles (HF), MOLL gland (MOLL), conjunctiva (CON), submucosa (SUBM), sub cutis (SC), blood (BL), levator aponeurosis (LAPO), skeletal muscle (SKM), epidermal basal cells (EPI-B), EPI-S, immune cell-enriched tissues (IC-1 and IC-2), and dermal cells (DE/DE-1).

maintenance and lipid metabolism, indicating that certain functions are shared across adnexal glands.

Functional enrichment highlights metabolic and secretory specialization

GO enrichment analyses further clarified the biological functions of the Moll gland transcriptional programs (Fig. 2D). The ST markers were significantly enriched for the GO terms "small molecule metabolism" (GO:0044281), "extracellular exosome" (GO:0070062), and "4-phosphate/phosphoenolpyruvate-family amino acid metabolism" (GO:1902221). Similarly, the SOM-derived set of 28 co-regulated genes, which included 10 genes shared with the ST markers, showed significant enrichment for "medium-chain fatty acid metabolism" (GO:0051791) and "tyrosine metabolism"

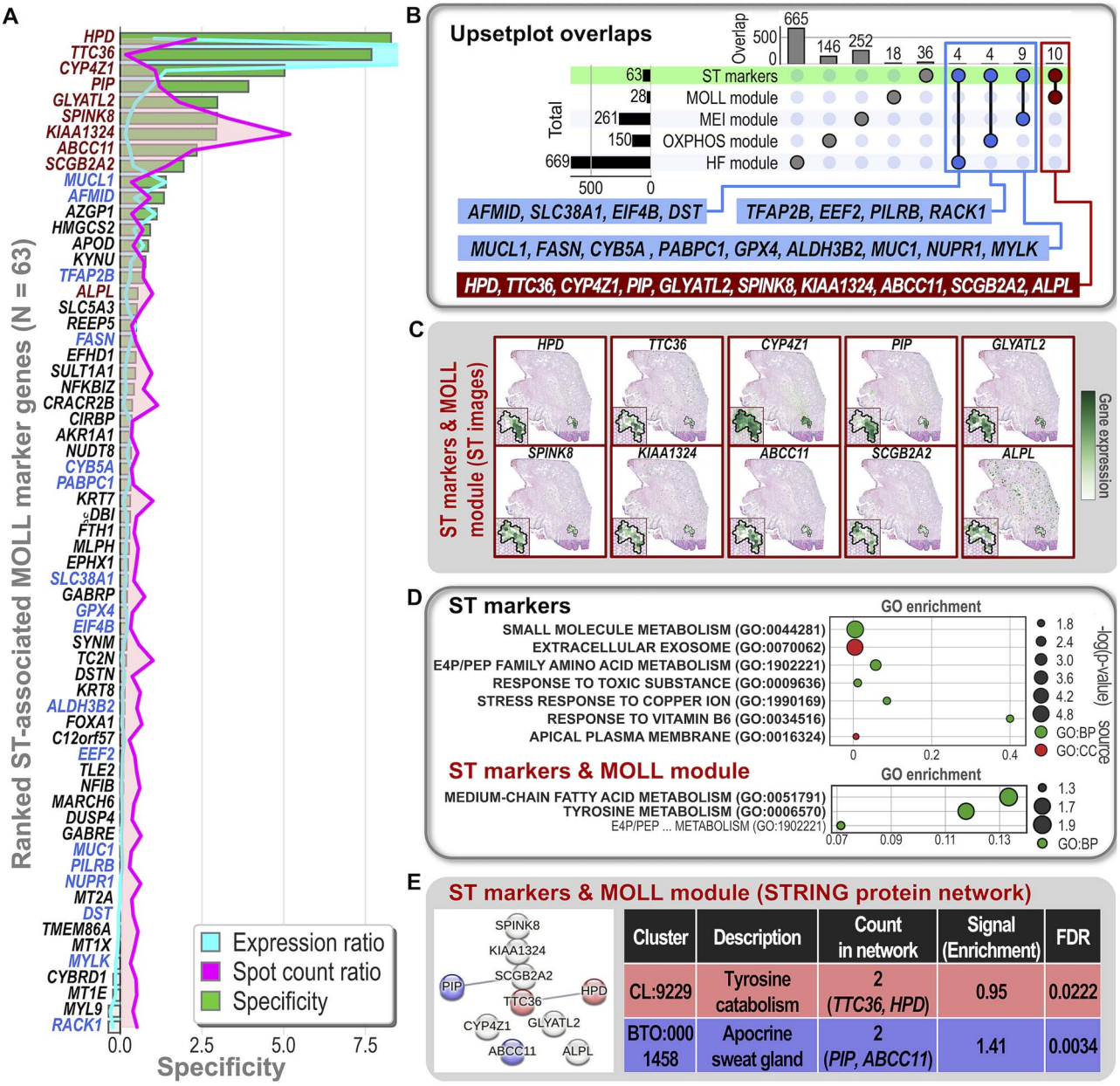

Figure 2 Annotation of ST markers. (A) Plot of all 63 MOLL-associated ST marker genes ranked by MOLL specificity score. (B) the Upsetplot illustrates the overlaps of ST markers, enabling the identification of "MOLL-only" gene signatures. Dark red labels indicate genes overlapping between ST markers and the MOLL module, while blue labels indicate genes overlapping between ST markers and the MEI, OXPHOS, and HF modules. The spatial expression patterns (C) of the "MOLL-only" gene signatures illustrate specific activation in the Moll gland. (D) GO enrichment analysis of ST markers genes and their overlaps with MOLL module gene sets. Enrichment (defined as the size of the intersection divided by the size of the GO term) is presented for the most significantly enriched GO terms. Legend: Dot size corresponds to -$\log_{10}$(p-value), dot color corresponds to the GO database source. Highlighted GO terms were defined by the g:Profiler (g:GOSt) tool and are preferentially shown. E4P: Erythrose 4-phosphate; PEP: Phosphoenolpyruvate. (E) Protein network clustering by STRING shows two distinct clusters, each consisting of two nodes (genes), accompanied by a table listing enriched STRING terms for each cluster.

(GO:0006570), and a weaker enrichment for "4-phosphate/phosphoenolpyruvate-family amino acid metabolism" (GO:1902221). Additionally, STRING network analysis (Fig. 2E) revealed two distinct clusters, namely "Tyrosine catabolism" (CL:9229) and "Apocrine sweat gland" (BTO:0001458).

For an extended view, gene sets from independent publications were also considered, as collected in the Molecular Signatures Database (MSigDB) [25] and implemented in the oposSOM software [17]. MOLL genes were significantly enriched in multiple breast cancer-related gene sets, most prominently those associated with the molecular apocrine subtype (Table 1 and Supplementary Table S1), which is characterized by androgen receptor signaling and FOXA1-mediated transcriptional regulation [26–28]. Genes overlapping between the gene sets and the MOLL module include *ABCC11*, *CYP4Z1*, *KIAA1324*, *PIP*, *SCGB1D2*, and *KAZALD1*. They converge on apocrine gland related functions such as lipid metabolism, secretion, and innate immune defense. *ABCC11* encodes a membrane transporter linked to apocrine gland activity and body odor formation [29], while *CYP4Z1*

Table 1 MSigDB gene sets enriched in the MOLL module.

Gene set name	# genes/# genes in Moll	*P*-value	Reference
LIEN BREAST CARCINOMA METAPLASTIC VS DUCTAL DN	104/5	1.13E-08	[26]
DOANE BREAST CANCER ESR1 UP	105/3	2.39E-05	[27]
SMID BREAST CANCER RELAPSE IN BONE UP	92/2	4E-04	[28]
SMID BREAST CANCER BASAL DN	643/5	3E-04	[28]

encodes a fatty acid hydroxylase involved in lipid oxidation [30]. KAZALD1 is a secreted protein localized in secretory odontoblasts [31], and SCGB1D2 is a lipophilin subfamily member with antimicrobial activity [32]. *KIAA1324* is an estrogen induced gene associated with secretory tissues such as salivary glands and with endosome lysosome autophagy [33, 34], whereas PIP is detected in various bodily fluids including milk, saliva, and sweat and acts as a protective factor in innate immunity [35]. The consistent presence of these genes across independent gene sets supports a conserved transcriptional program linked to apocrine differentiation rather than to general epithelial proliferation.

Collectively, the results indicate that MOLL-associated gene sets exhibit distinct but complementary functional programs, reflecting the gland's specialized metabolic capacity and secretory function within the eyelid tissue microenvironment.

Immunofluorescence confirms GLYATL2 and HPD as novel *bona fide* markers of the Moll gland

Among the 10 genes defining the Moll gland (Fig. 2B and C), only PIP (prolactin-induced protein) has already been reported to be expressed in these structures [36], and PIP levels are reduced in patients with keratoconus, a degenerative disease of the cornea [37]. To confirm that further transcripts detected as typical for the Moll gland are present as proteins, we selected GLYATL2 and HPD, two functionally distinct transcripts meeting the specificity criteria (see Fig. 2A–C) for validation by immunofluorescence. GLYATL2 is a poorly characterized transferase that produces N-acyl glycines in humans [38], while HPD is a key enzyme of tyrosine catabolism [39]. We detected a strong and specific staining for both GLYATL2 and HPD in cells of the Moll gland in the eyelid sample employed for ST analysis (Fig. 3A and E) as well as in eyelids from three additional patients (Fig. 3B–D and 3F–H). Negative controls omitting the primary antibody showed no staining (not shown).

Discussion and conclusion

Although they have been known to researchers since the 19th century [9, 40], our knowledge about the Moll glands of the eyelid remains essentially restricted to anatomical features and to the expression of a few membrane proteins [10, 11] and secretory products [12, 13]. Moll glands are likely to play an important role in the eyelid health and therefore in securing adequate visual function, but the exact mechanisms remain unknown [9]. Finally, Moll gland dysfunction results in ocular pathologies such as eyelid hidrocystomas [41].

Departing from spatial transcriptome data, we employed a range of bioinformatic tools built around machine learning using SOM portrayal to pinpoint the transcriptional program of the Moll glands and compare it to other glandular structures of the eyelid. While a number of platforms for assessing and visualizing spatial transcriptome data are available [42, 43], our method offers "portrayal advantage" meaning that it provides the local expression landscape of each spatial spot as an easy-to-percept image that enables segmentation into functional modules and gene-level analysis. This advantage partly overcomes the limited resolution of the 10x Genomics standard VISIUM technology by enabling to extract mixed cell-type compositions in the spots. Researchers can thus interactively browse the microanatomy of the glands using the spatial browser to address questions beyond the results presented in this publication. The relative expression patterns highlight how glandular tissues differ in their predominant biological pathways: lipid and energy (OXPHOS) metabolism is strongly associated with Meibomian [7] and sebaceous glands [15, 44], consistent with their secretory role in stabilizing the tear film and protecting the eyelid surface and eyelashes, respectively. Conversely, RNA processing modules upregulate across many tissues, first of all within the HF cluster, reflecting the high proliferative dynamics of follicular epithelial cells [45]. Thus, these functional modules align with the tasks of each structure, confirming that transcriptional signatures directly reflect tissue physiology.

In addition to these functions shared with other tissues of the eyelid, the Moll gland reveals distinct functional themes such as tyrosine metabolism, possibly related to antimicrobial peptide functions, and apocrine gland membrane transport and secretion, which are virtually absent in the other tissues. Interestingly, SOM portrayal identified MOLL-specific genes as a separate module expressed in the spatially resolved transcriptional portraits of the MOLL spots. Hence, the gland of Moll demonstrates a unique expression pattern, placing it transcriptionally between epidermal and adnexal epithelia.

The SOM mapping demonstrates that ocular adnexal glands are not isolated units but part of a highly coordinated system. Each structure maintains its transcriptional identity while contributing to the wider epithelial and immune environment of the ocular surface. The immune cell clusters bridging epithelial and submucosal compartments further emphasize the integration of barrier defense and secretory function. Taken together, these data establish a foundational framework for understanding how glandular diversity supports ocular surface homeostasis in general and sheds light on the transcriptional landscape of the largely neglected Moll gland. The identification of Moll gland-related genes in this study relies on spatial transcriptomics combined with SOM-based molecular portrayal and cluster-based marker detection combined with a specificity score to distinguish genes expressed almost exclusively in the Moll gland and genes also expressed in other tissues. While this integrated approach enables spatially resolved module-level analysis, it has limitations that should be considered when interpreting the results and motivate future studies using higher-resolution and multi-sample datasets. First, the spatial resolution of the Visium platform does not resolve individual cells, and each spot typically captures transcripts from multiple adjacent cell types, potentially diluting cell-type-specific signals. Second, lowly expressed genes or transcripts restricted to very

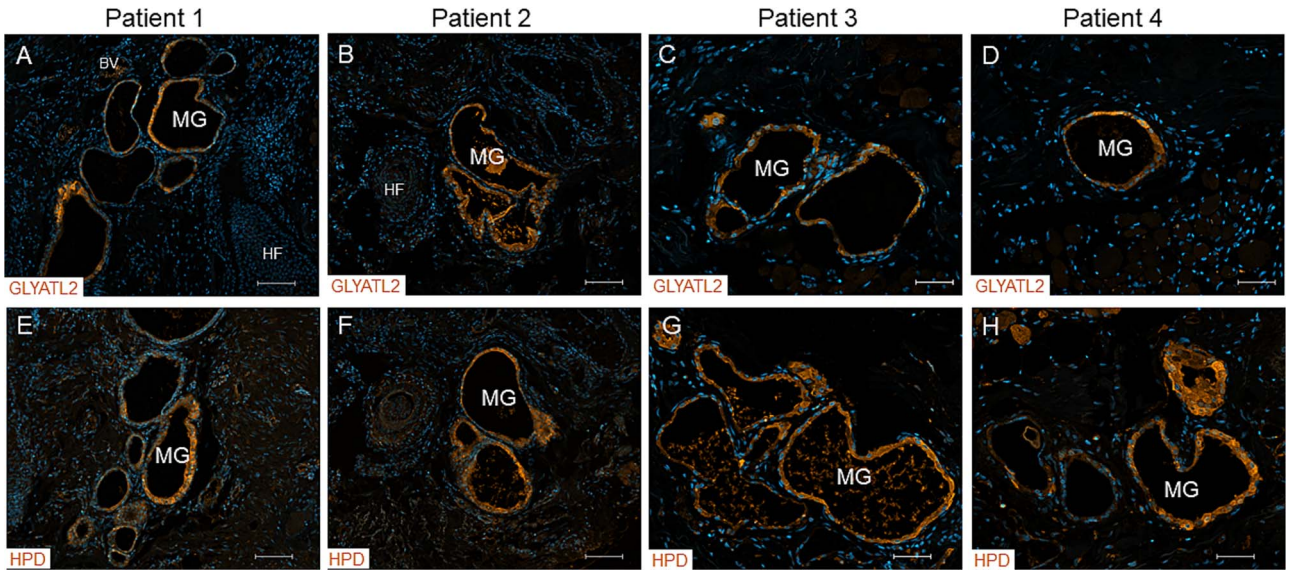

Figure 3 Expression of GLYATL2 in Moll glands. (A) Immunofluorescence detection of GLYATL2 (A–D) and HPD (E–H) (both in orange, stained with Cy3) in human Moll glands (MG). Nuclei are stained with DAPI. Scale bar represents 50 μm (C, D, G, H) or 100 μm (A, B, E, F). BV: Blood vessel, HF: Hair follicle.

small cellular subpopulations may remain undetected due to filtering and spot-level averaging. Third, our results and their interpretation are largely based on GO enrichment and network analyses, which provide reasonable but indirect evidence for specialized metabolic and secretory roles of the Moll gland. Finally, a limitation of the current study (but not of the approach in general) is that the analysis is based on a single human eyelid specimen, enabling a unique case study but lacking information about inter-individual variability, e.g. in the context of aging and/or diseases. This drawback is in part overcome by the validation of two markers in the eyelids of four different patients.

On a broader note, our study underscores the power of ST data to identify and characterize rare cell types within complex, microstructured tissues [46–48]. We demonstrate that ST integrated with machine learning allows generating a fine-grained portrait of the transcriptional landscape of such cells even when the source data are of relatively low resolution, such as those obtained from standard Visium analysis.

Key Points

- Moll glands are an important but largely neglected component of the eyelid.
- Moll glands emerge as a separate cell cluster in a spatial transcriptome analysis of the human eyelid.
- We employ a range of bioinformatic tools to characterize the transcriptional landscape of Moll gland cells.
- Moll gland-associated gene sets reflect the gland's specialized metabolic capacity and secretory function within the eyelid microenvironment.

Acknowledgments

Supported by the Open Access Publishing Fund of Leipzig University.

Author contributions

Hans Binder (Conceptualization, Data curation, Software, Validation, Visualization, Writing—original draft, Writing—review & editing), Marlon R. Schneider (Conceptualization, Validation, Writing—review & editing), Tomas Konecny (Data curation, Software, Validation, Visualization, Writing—original draft, Writing—review & editing), Helga Pfannkuche (Data curation, Validation, Writing—review & editing), Ulrike Hampel (Validation, Writing—review & editing), and Florian Hansmann (Validation, Writing—review & editing)

Supplementary material

Supplementary material is available at *Briefings in Bioinformatics* online.

Conflict of interest

The authors declare that they have no conflict of interest.

Funding

H.B. and T.K. acknowledge the support of the Higher Education and Science Committee of the Republic of Armenia in the frame of the project 25RL-1F024F005.

Data availability

Datasets related to this article can be found at the public Leipzig Health Atlas repository (https://www.health-atlas.de) under the accession number LHA ID:8MWXC02K01–6. Together with this publication, we provide an interactive web browser for inspecting the ST data of the eyelid (http://gondwanaland.izbi.uni-leipzig.de:5978/?dataset=17).

Ethics approval

The eyelid samples employed in this study were collected at the Department of Ophthalmology of the University of Leipzig during

lateral tarsal strip procedure for ectropion correction and after patient consent for use of the specimen for research purposes, and in full compliance with the Declaration of Helsinki principles.

References

1. Pflugfelder SC, Stern ME. Biological functions of tear film. *Exp Eye Res* 2020;**197**:108115. https://doi.org/10.1016/j.exer.2020.108115
2. Bannier-Hélaouët M, Post Y, Korving J *et al.* Exploring the human lacrimal gland using organoids and single-cell sequencing. *Cell Stem Cell* 2021;**28**:1221–1232.e7. https://doi.org/10.1016/j.stem.2021.02.024
3. Mauduit O, Delcroix V, Umazume T *et al.* Spatial transcriptomics of the lacrimal gland features macrophage activity and epithelium metabolism as key alterations during chronic inflammation. *Front Immunol* 2022;**13**:1011125. https://doi.org/10.3389/fimmu.2022.1011125
4. Butovich IA, Wilkerson A. Dynamic changes in the gene expression patterns and lipid profiles in the developing and maturing Meibomian glands. *Int J Mol Sci* 2022;**23**:7884. https://doi.org/10.3390/ijms23147884
5. Wiedemann J, Kashgari G, Lane S *et al.* The effects of age and dysfunction on meibomian gland population dynamics. *Ocul Surf* 2024;**34**:194–209. https://doi.org/10.1016/j.jtos.2024.08.005
6. Zhu X, Xu M, Portal C *et al.* Identification of Meibomian gland stem cell populations and mechanisms of aging. *Nat Commun* 2025;**16**:1663. https://doi.org/10.1038/s41467-025-56907-6
7. Binder H, Hampel U, Loeffler-Wirth H *et al.* Spatial transcriptome analysis of the human eyelid depicts meibomian gland cell differentiation: a pilot study. *Physiol Rep* 2025;**13**:e70571. https://doi.org/10.14814/phy2.70571
8. Yeu E, Garg S, Ayres BD *et al.* Current state and future perspectives in the diagnosis of eyelid margin disease: clinical review. *J Cataract Refract Surg* 2024;**50**:868–75. https://doi.org/10.1097/j.jcrs.0000000000001483
9. Stopfer M, Zahn I, Jüngert K *et al.* Glands of Moll: history, current knowledge and their role in ocular surface homeostasis and disease. *Prog Retin Eye Res* 2025;**106**:101362. https://doi.org/10.1016/j.preteyeres.2025.101362
10. Karbanová J, Missol-Kolka E, Fonseca A-V *et al.* The stem cell marker CD133 (Prominin-1) is expressed in various human glandular epithelia. *J Histochem Cytochem* 2008;**56**:977–93. https://doi.org/10.1369/jhc.2008.951897
11. Jäger F, Paulsen F, Bergua A *et al.* Urea transporter-B expression on the ocular surface and in the lacrimal glands. *Ann Anat* 2022;**243**:151954. https://doi.org/10.1016/j.aanat.2022.151954
12. Stoeckelhuber M, Stoeckelhuber BM, Welsch U. Human glands of Moll: histochemical and ultrastructural characterization of the glands of Moll in the human eyelid. *J Invest Dermatol* 2003;**121**:28–36. https://doi.org/10.1046/j.1523-1747.2003.12328.x
13. Stoeckelhuber M, Messmer EM, Schubert C *et al.* Immunolocalization of defensins and cathelicidin in human glands of Moll. *Ann Anat* 2008;**190**:230–7. https://doi.org/10.1016/j.aanat.2007.12.001
14. Schmidt M, Avagyan S, Reiche K *et al.* A spatial transcriptomics browser for discovering gene expression landscapes across microscopic tissue sections. *Curr Issues Mol Biol* 2024;**46**:4701–20. https://doi.org/10.3390/cimb46050284
15. Schmidt M, Hansmann F, Loeffler-Wirth H *et al.* A spatial portrait of the human sebaceous gland transcriptional program. *J Biol Chem* 2024;**300**:107442. https://doi.org/10.1016/j.jbc.2024.107442
16. Ntranos V, Yi L, Melsted P *et al.* A discriminative learning approach to differential expression analysis for single-cell RNA-seq. *Nat Methods* 2019;**16**:163–6. https://doi.org/10.1038/s41592-018-0303-9
17. Löffler-Wirth H, Kalcher M, Binder H. oposSOM: R-package for high-dimensional portraying of genome-wide expression landscapes on bioconductor. *Bioinf (Oxf)* 2015;**31**:3225–7. https://doi.org/10.1093/bioinformatics/btv342
18. Binder H, Hopp L, Lembcke K *et al.* Personalized disease phenotypes from massive OMICs data. In: Wang B, Li R, Perrizo W (eds.), *Big Data Analytics in Bioinformatics and Healthcare*, pp. 359–78. Hershey, Pennsylvania (701 E. Chocolate Avenue, Hershey, Pa., 17033, USA): IGI Global. https://doi.org/10.4018/978-1-4666-6611-5.ch015.
19. Wirth H, von BM, Binder H. Mining SOM expression portraits: feature selection and integrating concepts of molecular function. *BioData Min* 2012;**5**:18. https://doi.org/10.1186/1756-0381-5-18
20. Wirth H, Löffler M, von BM *et al.* Expression cartography of human tissues using self organizing maps. *BMC Bioinformatics* 2011;**12**:306. https://doi.org/10.1186/1471-2105-12-306
21. Lex A, Gehlenborg N, Strobelt H *et al.* UpSet: visualization of intersecting sets. *IEEE Trans Vis Comput Graph* 2014;**20**:1983–92. https://doi.org/10.1109/TVCG.2014.2346248
22. Raudvere U, Kolberg L, Kuzmin I *et al.* G:profiler: a web server for functional enrichment analysis and conversions of gene lists (2019 update). *Nucleic Acids Res* 2019;**47**:W191–8. https://doi.org/10.1093/nar/gkz369
23. Reimand J, Kull M, Peterson H *et al.* G:profiler–a web-based toolset for functional profiling of gene lists from large-scale experiments. *Nucleic Acids Res* 2007;**35**:W193–200. https://doi.org/10.1093/nar/gkm226
24. Szklarczyk D, Kirsch R, Koutrouli M *et al.* The STRING database in 2023: protein-protein association networks and functional enrichment analyses for any sequenced genome of interest. *Nucleic Acids Res* 2023;**51**:D638–46. https://doi.org/10.1093/nar/gkac1000
25. Subramanian A, Tamayo P, Mootha VK *et al.* Gene set enrichment analysis: a knowledge-based approach for interpreting genome-wide expression profiles. *Proc Natl Acad Sci USA* 2005;**102**:15545–50. https://doi.org/10.1073/pnas.0506580102
26. Lien HC, Hsiao YH, Lin YS *et al.* Molecular signatures of metaplastic carcinoma of the breast by large-scale transcriptional profiling: identification of genes potentially related to epithelial-mesenchymal transition. *Oncogene* 2007;**26**:7859–71. https://doi.org/10.1038/sj.onc.1210593
27. Doane AS, Danso M, Lal P *et al.* An estrogen receptor-negative breast cancer subset characterized by a hormonally regulated transcriptional program and response to androgen. *Oncogene* 2006;**25**:3994–4008. https://doi.org/10.1038/sj.onc.1209415
28. Smid M, Wang Y, Zhang Y *et al.* Subtypes of breast cancer show preferential site of relapse. *Cancer Res* 2008;**68**:3108–14. https://doi.org/10.1158/0008-5472.CAN-07-5644
29. Brown S. The pharmacogenetics of body odor: as easy as ABCC? *J Invest Dermatol* 2013;**133**:1709–11. https://doi.org/10.1038/jid.2013.14
30. Kowalski JP, Rettie AE. There and Back again: a perspective on 20 years of CYP4Z1. *Drug Metab Dispos* 2024;**52**:498–507. https://doi.org/10.1124/dmd.124.001670
31. Feleke M, Feng W, Rothzerg E *et al.* Single-cell RNA-seq identification of four differentially expressed survival-related genes by a TARGET: osteosarcoma database analysis. *Exp Biol Med (Maywood)* 2022;**247**:921–30. https://doi.org/10.1177/15353702221080131
32. Strausz S, Abner E, Blacker G *et al.* SCGB1D2 inhibits growth of Borrelia burgdorferi and affects susceptibility to Lyme disease. *Nat Commun* 2024;**15**:2041. https://doi.org/10.1038/s41467-024-45983-9
33. Deng L, Feng J, Broaddus RR. The novel estrogen-induced gene EIG121 regulates autophagy and promotes cell survival under stress. *Cell Death Dis* 2010;**1**:e32. https://doi.org/10.1038/cddis.2010.9

34. Ohara Y, Liu H, Craig AJ *et al.* ELAPOR1 induces the classical/progenitor subtype and contributes to reduced disease aggressiveness through metabolic reprogramming in pancreatic cancer. *Int J Cancer* 2024;**155**:569–81. https://doi.org/10.1002/ijc.34960
35. Hou S, Wang X, Chen D *et al.* The secreted peptide PIP1 amplifies immunity through receptor-like kinase 7. *PLoS Pathog* 2014;**10**:e1004331. https://doi.org/10.1371/journal.ppat.1004331
36. Viacava P, Naccarato AG, Bevilacqua G. Spectrum of GCDFP-15 expression in human fetal and adult normal tissues. *Virchows Arch* 1998;**432**:255–60. https://doi.org/10.1007/s004280050163
37. Sharif R, Bak-Nielsen S, Sejersen H *et al.* Prolactin-induced protein is a novel biomarker for keratoconus. *Exp Eye Res* 2019;**179**:55–63. https://doi.org/10.1016/j.exer.2018.10.015
38. Waluk DP, Schultz N, Hunt MC. Identification of glycine N-acyltransferase-like 2 (GLYATL2) as a transferase that produces N-acyl glycines in humans. *FASEB J* 2010;**24**:2795–803. https://doi.org/10.1096/fj.09-148551
39. Moran GR. 4-Hydroxyphenylpyruvate dioxygenase. *Arch Biochem Biophys* 2005;**433**:117–28. https://doi.org/10.1016/j.abb.2004.08.015
40. Sattler H. Beitrag zur Kenntniss der modificirten (Moll'schen) Schweissdrüsen des Lidrandes. *Archiv f mikrosk Anat* 1877;**13**:783–95. https://doi.org/10.1007/BF02933957
41. Jakobiec FA, Zakka FR. A reappraisal of eyelid eccrine and apocrine hidrocystomas: microanatomic and immunohistochemical studies of 40 lesions. *Am J Ophthalmol* 2011;**151**:358–74.e2. https://doi.org/10.1016/j.ajo.2010.08.028
42. Zhang P, Chen W, Tran TN *et al.* Thor: a platform for cell-level investigation of spatial transcriptomics and histology. *Nat Commun* 2025;**16**:7178. https://doi.org/10.1038/s41467-025-62593-1
43. Li B, Tang Z, Budhkar A *et al.* SpaIM: single-cell spatial transcriptomics imputation via style transfer. *Nat Commun* 2025;**16**:7861. https://doi.org/10.1038/s41467-025-63185-9
44. Schmidt M, Binder H, Schneider MR. The metabolic underpinnings of sebaceous lipogenesis. *Commun Biol* 2025;**8**:670. https://doi.org/10.1038/s42003-025-08105-9
45. Schneider MR, Schmidt-Ullrich R, Paus R. The hair follicle as a dynamic miniorgan. *Curr Biol* 2009;**19**:R132–42. https://doi.org/10.1016/j.cub.2008.12.005
46. Jones ASK, Hannum DF, Machlin JH *et al.* Cellular atlas of the human ovary using morphologically guided spatial transcriptomics and single-cell sequencing. *Sci Adv* 2024;**10**:eadm7506. https://doi.org/10.1126/sciadv.adm7506
47. Cho H, Zhang Y, Tien JC *et al.* Cellular cartography reveals mouse prostate organization and determinants of castration resistance. *Proc Natl Acad Sci USA* 2025;**122**:e2427116122. https://doi.org/10.1073/pnas.2427116122
48. Sun ED, Zhou OY, Hauptschein M *et al.* Spatial transcriptomic clocks reveal cell proximity effects in brain ageing. *Nature* 2025;**638**:160–71. https://doi.org/10.1038/s41586-024-08334-8

Briefings in Bioinformatics, 2026, **27**, bbag135
https://doi.org/10.1093/bib/bbag135
Case Study